energies

MDPI

Article

Distributed PV Bearing Capacity Assessment Method Based on Source–Load Coupling Scenarios

Yalu Sun [1], Zhou Wang [1], Yongcheng Liu [1], Yi Jiang [2] and Yalong Li [2,*]

[1] Economic and Technological Research Institute, State Grid Gansu Electric Power Company, Lanzhou 730000, China; syl_gsdl@163.com (Y.S.); 13669338713@163.com (Z.W.); 18894039391@163.com (Y.L.)
[2] School of Mechanical and Electrical Engineering, China University of Mining and Technology-Beijing, Beijing 100083, China; 17861737758@163.com
* Correspondence: 201726@cumtb.edu.cn

Abstract

To address the insufficient consideration of system static voltage stability and PV–load coupling in distributed photovoltaic (PV) hosting capacity assessment, this study first investigates the impact of distributed PV integration on power system transient voltage stability based on a typical power supply system. Building on this analysis, we propose a Static Grid Stability Margin (SGSM) index. Subsequently, leveraging historical PV and load data, the copula function is introduced to establish a joint distribution function characterizing their correlation. Massive evaluation scenarios are generated through sampling, with robust clustering methods employed to form representative evaluation scenarios. Finally, a distributed PV bearing capacity assessment model is established with the objectives of maximizing PV bearing capacity, optimizing economic efficiency, and enhancing static voltage stability. Through simulation verification, the power system has a higher capacity for distributed PV when distributed PV is integrated into nodes with weak static voltage stability and a decentralized integration scheme is adopted.

Keywords: distributed photovoltaic; bearing capacity assessment; source–load coupling; static voltage stability



Academic Editor: Mario Russo

Received: 11 September 2025
Revised: 15 October 2025
Accepted: 16 October 2025
Published: 20 October 2025

Citation: Sun, Y.; Wang, Z.; Liu, Y.; Jiang, Y.; Li, Y. Distributed PV Bearing Capacity Assessment Method Based on Source–Load Coupling Scenarios. *Energies* **2025**, *18*, 5520. https://doi.org/10.3390/en18205520

Copyright: © 2025 by the authors. Licensee MDPI, Basel, Switzerland. This article is an open access article distributed under the terms and conditions of the Creative Commons Attribution (CC BY) license (https://creativecommons.org/licenses/by/4.0/).

1. Introduction

Due to the rapid development of distributed PV, power system operation is facing challenges [1–3]. With the deepening advancement of the new power system, renewable energy in China has developed explosively, particularly distributed PV, which has significantly increased the proportion of clean energy consumption [4]. However, due to climate factors such as cloud cover, the output of distributed PV exhibits significant fluctuations and randomness, which poses severe challenges to the safe and stable operation of the power grid [5]. On one hand, the large-scale integration of distributed PV has altered the operational landscape of the power grid, transforming traditional distribution grids from purely receiving-end grids to a grid that integrates power generation and consumption, where an excessive reverse load rate can severely impact grid safety. On the other hand, the variability of distributed PV output can affect voltage quality, voltage stability, harmonic content, etc. The unrestricted connection of distributed PV would inevitably lead to a deterioration in grid safety [6,7]. Distributed PV bearing capacity refers to the maximum capacity that the grid can accommodate while meeting all operational constraints of the power system and equipment. So, distributed PV bearing capacity assessment is of critical importance.

Regarding the assessment of distributed PV bearing capacity, some scholars have already conducted relevant research. They mainly focus on the key factors caused by distributed PV integration into distribution grids, such as reverse load rate and voltage deviation, extracting relevant constraint indicators for evaluation. References [8–11] establish a distributed PV bearing capacity assessment model for distribution grids by considering multi-constraint conditions, with the objective of maximizing the PV capacity that the grid can accommodate; reference [12] considers the feed-end bus voltage and constructs an evaluation of the access capacity of distributed PV; and references [13–16] realize the evaluation and calculation of the PV capacity through various algorithms.

The above method provides an effective approach for the assessment of distributed photovoltaic (PV) capacity. However, it does not take into account the impact of static voltage stability. References [17–19] calculate the static voltage stability boundary based on fixed scenarios or operating states and then use the boundary as a constraint to assess the distributed PV capacity. Nevertheless, the system's static voltage stability is closely related to the system's operating state and the penetration level of distributed PV—specifically, the penetration level of distributed PV and static voltage stability are tightly coupled. It is necessary to consider the impact of changes in the static voltage stability boundary with the power grid's operating modes, which has not yet been studied. Meanwhile, the bearing capacity is closely related to the grid operation mode. For example, in grids with heavy loads, the integration of distributed PV can effectively reduce transformer-side power flow, thereby benefiting grid safety. However, when the capacity of distributed PV exceeds a certain proportion, it may face the dual challenges of excessive reverse power flow during periods of low load and heavy PV generation, as well as excessive forward power flow during evening peak load periods when PV generation is absent. Additionally, significant fluctuations in power flow throughout the day pose a severe challenge to the safe and stable operation of the power grid. Therefore, distributed PV bearing capacity assessment needs to be comprehensively judged in conjunction with the actual operating conditions of the grid [20,21]. To account for the impact of the source–load coupling characteristic, references [22,23] consider the coordinated operation of various regulatory resources within the grid, such as smart inverters and model predictive controllers, to improve distributed PV bearing capacity. References [24–27] describe the correlation between photovoltaic (PV) output and load based on the copula function and use sampling methods to extract different typical scenarios. Distributed PV capacity assessment is conducted on this basis. However, when extracting typical scenarios, they ignore the issue that PV output has large fluctuations and may be affected by extreme weather data. For example, in a certain cluster, most data points are concentrated in a specific location, while a few points are relatively far from the center. In such cases, typical scenarios should be more inclined to the location where most data are gathered, and the impact of data points far from the center should be weakened. Reference [28] assesses the PV bearing capacity considering the uncertainty of source and load by the random optimization method.

Based on the above analysis, current research on the assessment of distributed photovoltaic (PV) capacity is relatively well developed, but there are still two aspects that need improvement: Firstly, regarding the consideration of static voltage stability, at present, the static voltage stability boundary is mostly calculated based on fixed scenarios or operating states and cannot dynamically change with the system's operating state or the penetration level of distributed PV. This poses a risk that the capacity assessment results may exceed the stability boundary. Secondly, in the generation of source–load-coupled scenarios, some individual data points (not abnormal data but can be understood as atypical cases of normal output, which often occur in PV output scenarios with large fluctuations) are relatively

far from the center. This causes the typical scenarios obtained through clustering to fail to reflect the majority of cases, leading to deviations in capacity assessment.

To address the above issues, this paper makes the following contributions:

(1) It extracts static voltage stability indicators that take distributed PV integration into account. These indicators can dynamically change according to different PV penetration levels, and optimization is conducted based on them. Compared with the current static voltage stability boundary calculated based on fixed scenarios or operating states, this approach is more accurate.

(2) It proposes a weighted-variable K-Means algorithm. When updating the cluster center, weight coefficients are calculated based on Euclidean distance—data points with a larger Euclidean distance are assigned a smaller weight coefficient. This helps mitigate the impact of outliers on clustering results.

(3) It establishes a multi-objective assessment model for distributed PV capacity and conducts simulation verification based on measured data. Conclusions are drawn, such as the following: when distributed PV is integrated into nodes where the system's static voltage stability is weak, the system can accommodate more distributed PV.

2. Extraction of Static Voltage Stability Factors in the Grid for Distributed PV Integration

Voltage stability issues in the grid typically occur at the end nodes of the load. Upstream of the load node, there is always one or more power supply nodes. Centered on the load node, the local grid can always be equivalently modeled as the lattice structure shown in Figure 1. Based on this system, the impact of distributed PV integration on the static voltage stability of the power grid is derived.

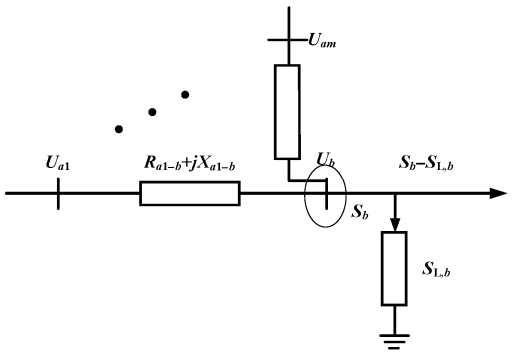


Figure 1. Multi-infeed Node Branch Model.

In Figure 1, node b denotes a load node; S_b and $S_{L,b}$ denote the power flowing through node b and the load power, respectively; and $R_{am\text{-}b}$ and $X_{am\text{-}b}$ denote the line resistance and reactance, respectively. The black dots represent the abbreviated notation from node $a1$ to node am.

2.1. Extraction of Static Voltage Stability Prior to Distributed PV Integration

Taking branch am-b as an example for analysis, the voltage between node am and node b satisfies

$$U_{am}\angle\delta_{am} = U_b\angle\delta_b + \frac{(R_{am\text{-}b} + jX_{am\text{-}b})(P_{am\text{-}b} - jQ_{am\text{-}b})}{U_b\angle -\delta_b} \quad (1)$$

where U_{am} and U_b denote the voltages of node am (the m-th node connected to node b) and node b, respectively; δ_{am} and δ_b denote the phase angles of node am and node b, respectively; $R_{am\text{-}b}$ and $X_{am\text{-}b}$ denote the resistance and reactance of branch am-b (the m-th branch connected to node b), respectively; and $P_{am\text{-}b}$ and $Q_{am\text{-}b}$ denote the active power and

reactive power of branch *am-b* (the *m*-th branch connected to node *b*), respectively, which satisfy Kirchhoff's laws with respect to the power of node *b*, namely:

$$P_{am-b} + jQ_{am-b} = \frac{\dfrac{1}{R_{am-b} + jX_{am-b}}}{\sum\limits_{k=1}^{K} \dfrac{1}{R_{ak-b} + jX_{ak-b}}}(P_b + jQ_b) \Rightarrow$$
$$\begin{cases} P_{am\text{-}b} = \mathrm{Re}\left(\dfrac{1}{(R_{am-b} + jX_{am-b}) \sum\limits_{k=1}^{K} \dfrac{1}{R_{ak-b} + jX_{ak-b}}}(P_b + jQ_b) \right) \\ Q_{am\text{-}b} = Qe\left(\dfrac{1}{(R_{am-b} + jX_{am-b}) \sum\limits_{k=1}^{K} \dfrac{1}{R_{ak-b} + jX_{ak-b}}}(P_b + jQ_b) \right) \end{cases} \tag{2}$$

where K is the total number of nodes connected to node b. P_b and Q_b are the injected active power and reactive power of node b, respectively.

For ease of exposition, Formula (2) can be expressed as a function of the active and reactive power injected at node b, as follows:

$$\begin{cases} P_{am\text{-}b} = f_p(P_b, Q_b) \\ Q_{am\text{-}b} = f_q(P_b, Q_b) \end{cases} \tag{3}$$

Combining Formulas (1) and (3), and assuming that the phase angle of the voltage at node b is 0°, Formula (1) can be further simplified to

$$\begin{aligned} & U_{am} = U_b + \tfrac{(R_{am\text{-}b} + jX_{am\text{-}b})(P_{am\text{-}b} - jQ_{am\text{-}b})}{U_b} \\ & \Rightarrow U_b^4 - \left(U_{am}^2 - 2M\right)U_b^2 + M^2 + N^2 = 0 \\ & \begin{cases} M = f_p(P_b, Q_b)R_{am\text{-}b} + f_q(P_b, Q_b)X_{am\text{-}b} \\ N = f_p(P_b, Q_b)X_{am\text{-}b} - f_q(P_b, Q_b)R_{am\text{-}b} \end{cases} \end{aligned} \tag{4}$$

where M and N are intermediate variables of the simplified formula, with no actual physical meaning.

From the above formulas, it follows that the voltage stability equation for node b satisfies a quadratic relationship. If the voltage at node b is stable, it indicates that Formula (4) possesses real solutions. Similarly, if Formula (4) possesses real solutions, it shows that a voltage exists at node b under any operating condition; thus, the voltage at node b is stable. Formula (4) having real solutions is equivalent to the voltage at node b being stable. Therefore,

$$\begin{aligned} & \Delta = \left(U_{am}^2 - 2M\right)^2 - 4\left(M^2 + N^2\right) \geq 0 \\ & \Rightarrow U_{am}^4 \geq 4\left(MU_{am}^2 + N^2\right) \end{aligned} \tag{5}$$

In the actual operation of power grids, due to $U_{am}^4 > 0$,

$$\frac{4\left(MU_{am}^2 + N^2\right)}{U_{am}^4} \leq 1 \tag{6}$$

Therefore, the stability of the voltage at node b is equivalent to Formula (6).

Consequently, the stability index $L_{\mathrm{SVS},am\text{-}b}$ for node b in branch *am-b* can be defined as

$$L_{\mathrm{SVS},am\text{-}b} = \frac{4[MU_{am}^2 + N^2]}{U_{am}^4} \tag{7}$$

The smaller $L_{SVS,am\text{-}b}$ is, the greater the static voltage stability margin at node b. When $L_{SVS,am\text{-}b}$ exceeds 1, voltage instability will begin at node b.

The static voltage stability of node b is determined by the worst-performing supply branch among all supply branches. The voltage stability index $L_{SVS,b}$ for node b is defined as

$$L_{SVS,b} = \max_{b=1:K}(L_{SVS,ak-b}) \tag{8}$$

In the same vein, the static voltage stability of the entire system is determined by the worst-case node, and, thus, the static voltage stability of the entire system is

$$L_{SVS,s} = \max_{k}(L_{SVS,k}) \tag{9}$$

The detailed derivation process is shown in the Appendix A.

From Formula (7), it is known that when the grid structure remains unchanged, i.e., the resistance and reactance parameters do not change, the static voltage stability at node b is primarily related to the magnitude of the load (active and reactive power) at node b. After distributed PV is connected to node b, the net load at node b is inevitably altered, thereby affecting the voltage stability of both node b and the system.

2.2. Extraction of Grid Static Voltage Stability Factors Following Distributed PV Integration

After distributed PV is connected to node b, the power output of node b becomes

$$S_b = (P_{b,L} - P_{b,PV}) + k(Q_{b,L} - Q_{b,PV}) \tag{10}$$

Typically, to ensure economic efficiency, photovoltaic inverters operate at a power factor of 1. Therefore, $Q_{b,PV} = 0$. Referring to Formula (7), where the node b power in parameters M and N is replaced by the power from Formula (10), the voltage stability indicator $L_{SVS,am\text{-}b}$ for node b in the base branch am-b is updated as follows:

$$\begin{aligned} &L_{SVS,am\text{-}b} = \frac{4[MU_{am}^2+N^2]}{U_{am}^4} \\ &\begin{cases} M = f_p(P_{b,L} - P_{b,PV}, Q_b)R_{am\text{-}b} + f_q(P_{b,L} - P_{b,PV}, Q_b)X_{am\text{-}b} \\ N = f_p(P_{b,L} - P_{b,PV}, Q_b)X_{am\text{-}b} - f_q(P_{b,L} - P_{b,PV}, Q_b)R_{am\text{-}b} \end{cases} \end{aligned} \tag{11}$$

From Formula (2), it follows that M and N are linear functions of active and reactive power, respectively. Therefore, Formula (11) represents a quadratic function of power. Assuming the voltage operates near its rated value, i.e., $U_{am} \approx 1$, $L_{SVS,am\text{-}b}$ can be summarized as a quadratic function of photovoltaic active power:

$$L_{SVS,am\text{-}b} = q_1(P_b, Q_b)P_{PV}^2 - q_2(P_b, Q_b)P_{PV} + q_3(P_b, Q_b) \tag{12}$$

From Formula (12), it can be seen that when the grid's structural parameters and load power remain essentially unchanged, the system's static voltage stability margin exhibits a quadratic relationship with the photovoltaic active power, with an upward-opening curve. This indicates that after distributed PV integration to the system, the system's static voltage stability initially increases before decreasing, with the inflection point as follows:

$$P_{PV}^{lim} = \frac{q_2(P_b, Q_b)}{2q_1(P_b, Q_b)} \tag{13}$$

3. Source–Load Coupling Scenario Generation Method

Analysis of Section 2 reveals that the static voltage stability of the system is closely related to node load and photovoltaic output. As these two parameters fluctuate con-

tinuously during actual operation, a coupled analysis of load and photovoltaic output is required to better assess power grid bearing capability. Subsequently, typical output scenarios are categorized, with the maximum distributed PV hosting capacity under the most unfavorable scenario serving as the power grid bearing capability.

(1) Probability Modeling of Photovoltaic Output

As indicated in references [29–31], distributed PV output approximates a Beta distribution, with the probability density function $f(P_{PV})$ defined as

$$f(P_{PV}) = \frac{\Gamma(\varepsilon, \varphi)}{\Gamma(\varepsilon)\Gamma(\varphi)} \left(\frac{P_{PV}}{P_{PV}^{max}} \right)^{\varepsilon-1} \cdot \left(1 - \frac{P_{PV}}{P_{PV}^{max}} \right)^{\varphi-1} \tag{14}$$

where Γ denotes the gamma distribution and ε and φ are shape parameters, which can be obtained through fitting using historical photovoltaic data.

(2) Probabilistic Modeling of Load Output

As indicated in references [32–34], load data approximates a normal distribution with the following probability density function:

$$g(P_L) = \frac{1}{\sqrt{2\pi}\sigma_{PL}} \exp\left(-\frac{(P_L - \mu_{PL})^2}{2\sigma_{PL}^2} \right) \tag{15}$$

where P_L denotes the active power of the load and μ_{PL} and σ_{PL} denote the mean and standard deviation of the normal distribution, respectively.

(3) Coupled Output Modeling for Photovoltaic and Load

Photovoltaic output and load output constitute two random variables. Utilizing copula functions, their distribution functions can be described as a joint distribution function. Sampling based on this joint distribution function fully reflects the correlation between photovoltaic output and active load power. The specific steps are outlined below.

Step 1: Determine the marginal distributions of the two random variables: photovoltaic output and load output.

The marginal distribution functions of photovoltaic output and load power are, respectively,

$$\begin{cases} F(P_{PV}) = \int_{-\infty}^{P_{PV}} f(P_{PV}) \mathrm{d}t \\ G(P_L) = \int_{-\infty}^{P_L} f(g_L) \mathrm{d}t \end{cases} \tag{16}$$

Step 2: Select an appropriate copula function to combine the marginal distributions of two random variables into a multivariate distribution.

Common copula functions include the Gaussian copula, Frank copula, T-copula, Clayton copula, and Gumbel copula. Different copula functions describe distinct correlation patterns. The T-copula is better suited for handling distributions with heavy tails, while the Gaussian copula is appropriate for simulating correlations in normally distributed data. In practical implementation, the optimal copula function may be determined using the AIC (BIC) criterion, where lower values indicate superior performance. Based on this principle, the BIC values of various types of copula functions are shown in the table.

As can be seen from Table 1, the BIC value corresponding to the Frank copula function is the lowest, indicating that the Frank copula function is the best in describing the correlation between photovoltaic and load output. Therefore, this paper chooses the Frank copula function. By incorporating the distribution functions of photovoltaic output and

load power into the Frank copula function, the joint distribution function $H(F(P_{\mathrm{PV}}), G(P_{\mathrm{L}}))$ can be expressed as

$$H(F(P_{\mathrm{PV}}), G(P_{\mathrm{L}})) = -\frac{1}{\lambda}\ln\left[1+\frac{(e^{-\lambda F(P_{\mathrm{PV}})}-1)(e^{-\lambda G(P_{\mathrm{L}})}-1)}{e^{-\lambda}-1}\right] \tag{17}$$

where λ is the correlation parameter, which is the parameter to be estimated.

Table 1. BIC values of various types of copula functions.

Copula Function Type	BIC	Copula Function Type	BIC
Gaussian copula	603.5	Clayton copula	710.4
Frank copula	451.8	Gumbel copula	612.5
T-copula	555.2		

Step 3: Employ the maximum likelihood method to estimate the correlation parameter λ, thereby completing the calculation of the joint distribution.

Derive the probability density function of the joint distribution function $H(F(P_{\mathrm{PV}}), G(P_L))$, as shown below:

$$\begin{aligned} h(P_{\mathrm{PV}}, P_{\mathrm{L}}|\lambda) &= \frac{\partial H}{\partial P_{\mathrm{PV}}\partial P_L} \\ &= \frac{\partial H}{\partial F(P_{\mathrm{PV}})\partial G(P_{\mathrm{L}})}.f(P_{\mathrm{PV}}).g(P_{\mathrm{L}}) \end{aligned} \tag{18}$$

Let N be the sample size. The likelihood function is then given by

$$\begin{aligned} L(P_{\mathrm{PV}}, P_{\mathrm{L}}, \lambda) &= \prod_{i=1}^{N} h(P_{\mathrm{PV},i}, P_{\mathrm{L},i}|\lambda) \\ &= \prod_{i=1}^{n} h[F(P_{\mathrm{PV},i}), G(P_{\mathrm{L},i})|\lambda] f(P_{\mathrm{PV},i}).g(P_{\mathrm{L},i}) \end{aligned} \tag{19}$$

With the objective of maximizing the likelihood function as shown in Formula (17), the estimated value $\hat{\lambda}$ of the correlation parameter λ is obtained as follows:

$$\hat{\lambda} = \mathrm{argmax}\sum_{i=1}^{n} \ln[L(P_{\mathrm{PV}}, P_{\mathrm{L}}, \lambda)] \tag{20}$$

(4) Generation of Typical Scenarios Based on Clustering

Using the joint distribution function fitted via Formula (17), repeated sampling yields a substantial number of new photovoltaic and load output samples $(P'_{\mathrm{PV}}, P'_{\mathrm{L}})$. This approach essentially covers all practical operating modes, thus compensating for the shortcomings of insufficient actual sample data. Subsequently, the massive number of scenarios generated above are clustered into several typical scenarios, which are evaluated using the hosting capacity assessment. This paper employs an improved robust K-Means algorithm for clustering. The specific process is as follows:

Step 1: Initialize the cluster centers of K clusters, where K is the algorithm's hyper-parameter. This paper employs the silhouette coefficient method to determine the value of K. Its principle involves calculating the similarity a between the samples and its own cluster and the similarity b between the samples and the nearest other clusters. The silhouette coefficient s is, then, as follows:

$$s = \frac{|b-a|}{\max(a,b)} \tag{21}$$

The closer the coefficient is to 1, the better the clustering performance.

The average silhouette coefficient is computed for different K values, and the value of K corresponding to the maximum coefficient is chosen as the final number of clusters.

Step 2: Initial Assignment of Samples

The Euclidean distance is used to quantify the similarity between data samples, and each sample is assigned to its nearest cluster. Let the K clusters be represented as $\Omega_1, \Omega_2, \ldots, \Omega_K$, and their corresponding centers are $\mu_1, \mu_2, \ldots, \mu_K$. Then, the sample x satisfies

$$\begin{aligned} &x \in \Omega_m \\ &\|x - \mu_m\| \leq \min_{i=1:K, i \neq m} (\|x - \mu_i\|) \end{aligned} \tag{22}$$

Step 3: Update Cluster Centers

After the initial assignment of all samples, the mean of the samples within each cluster is taken as the new cluster center for re-clustering. The update formula of the cluster center is as follows:

$$\mu_m = \frac{1}{\|\Omega_m\|} \sum_{i \in \Omega_m} x_i \tag{23}$$

Step 4: Re-cluster using the updated cluster centers as the baseline until the change in cluster center updates falls below the threshold.

The aforementioned clustering process assumes that the data points are relatively uniformly distributed around cluster centers. But practical data analysis indicates that some data points may be away from cluster centers, which can significantly impact clustering results, as shown in the figure below.

In Figure 2, point A is relatively far away from the nodes of its cluster, and there is a possibility of anomaly. When updating and calculating the cluster center of the cluster, if the weight of point A is treated the same as that of other points, the cluster center may be shifted to point A, resulting in clustering deviation.

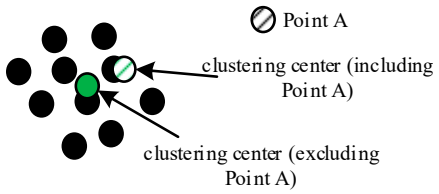


Figure 2. The impact of potential abnormal data on clustering results.

However, conventional K-Means algorithms cannot effectively handle this type of data. Therefore, building upon the original algorithm, this paper improves the traditional K-Means by proposing a variable-weight K-Means algorithm. This approach assigns lower weights to samples farther from the cluster center during the updating of cluster centers. The updated formula for cluster center calculation is transformed to

$$\begin{aligned} \mu_m &= \frac{1}{\|\Omega_m\|} \sum_{i \in \Omega_m} \omega_i x_i \\ \omega_i &= \frac{1}{1 + \|x - \mu_i\|^2} \end{aligned} \tag{24}$$

It can be seen that the farther a sample x_i is from the cluster center μ_m^{t-1} obtained in the previous iteration, the smaller its weight ω_i is. Consequently, the updated cluster center μ_m^t is less affected by possible outliers.

4. Bearing Capacity Assessment Method for Distributed PV in Multi-Level Power Supply Systems

The objective of this paper is to evaluate power grid bearing capability. As demonstrated by the preceding analysis, this capacity is closely tied to the degree of source–load coupling. If a strong positive correlation exists between the source and the load—meaning that during periods of high PV output, the load demand is also high—the electricity produced can be consumed locally, thereby enhancing distributed PV bearing capacity. Conversely, if there is a strong negative correlation—that is, when load demand is high, PV output is low, and when load demand is low, PV output is high—issues such as excessive voltage deviation at the end of the distribution network and a high reverse load rate are inevitably to arise. These adverse conditions hinder the improvement of distributed PV bearing capacity.

In Section 3, K typical source–load coupling output scenarios are generated, corresponding to K distinct source–load output curves. For the bearing capacity assessment, an optimization model is first established with the objectives of maximizing distributed PV hosting capacity, optimizing economic performance, and maximizing system static voltage stability. Then, sequential solutions are performed based on the source–load power curves under different scenarios. The assessment of the most critical scenario and the most vulnerable time instant (which could realistically occur) will be used as the final photovoltaic bearing capacity of the power grid.

4.1. Objective Function

Objective 1: Maximize the total distributed PV capacity connected at each grid node, expressed as

$$F_1 : \max \sum_{i=1}^{N} S_{k,t}^{PV} \tag{25}$$

where $S_{k,t}^{PV}$ denotes the distributed PV capacity connected at node i at time t in scenario k and N denotes the number of network nodes.

Objective 2: Following the integration of distributed PV into the system, it significantly alters the system power flow and affects the system line losses. The economic objective focuses on minimizing line losses. It is shown as follows:

$$\begin{aligned} F_2 : \min & \sum_{k,t=1}^{t=T} \left(P_{k,t}^{\mathrm{LOSS}} \cdot \Delta t \right) = \\ \min & \sum_{k,t=1}^{t=T} \left(\sum_{k,t=1}^{T} \sum_{i}^{N} |U_i| \sum_{j=1, j \neq i}^{N} |U_j| \left(G_{ij} \cos \theta_{ij} + B_{ij} \sin \theta_{ij} \right) \cdot \Delta t \right) \end{aligned} \tag{26}$$

where N denotes the number of nodes in the new energy power system; U_i denotes the voltage at node i; G_{ij} and B_{ij} denote the conductance and admittance of branch i-j, respectively; and θ_{ij} is the phase difference between node i and node j.

Objective 3: Maximizing System Static Voltage Stability

As the proportion of distributed PV generation increases, the system static voltage stability has become a primary constraint on the distributed PV bearing capacity. While meeting Objectives 1 and 2, it is also necessary to maximize static voltage stability after distributed PV integration:

$$F_3 : \min(L_{\mathrm{SVS},s}) = \min \left(\max_{k,t,i} (L_{\mathrm{SVS}}) \right) \tag{27}$$

It should be noted that integrating PV at different locations and capacities will lead to different weak points in the system (to be detailed in the simulation section later).

Therefore, when calculating the static voltage stability index shown in Formula (27), it must be recalculated whenever the integration scheme changes. However, this computation is relatively efficient. As indicated by Formula (27), the static voltage stability depends solely on network structure parameters and PV hosting capacity and not on the operational power flow of the system. Hence, once the PV integration scheme changes, algebraic calculations based on the updated PV capacity can be performed directly.

4.2. Constraints

For any scenario m at time t, the objective function must satisfy system power flow constraints, node voltage constraints, branch power flow constraints, and others. For simplicity, subscripts m and t are omitted in the following descriptions:

(1) System Power Flow Constraint

$$\begin{cases} P_{G,i} - P_{L,i} = U_i \sum_{j=1}^{n} U_j (G_{ij} \cos\theta_{ij} + B_{ij} \sin\theta_{ij}) \\ Q_{G,i} - Q_{L,i} = U_i \sum_{j=1}^{n} U_j (G_{ij} \cos\theta_{ij} - B_{ij} \sin\theta_{ij}) \end{cases} \tag{28}$$

Here, U_i denotes the voltage at node i; G_{ij} and B_{ij} denote the conductance and admittance of branch i-j, respectively; and θ_{ij} denotes the phase difference between nodes i and j.

(2) Node Voltage Constraint

According to GB/T 33593 [35], the maximum allowable voltage deviation in the grid is

$$\delta U(\%) = \frac{R_L P_{\max} + X_L Q_{\max}}{U_N^2} \tag{29}$$

where R_L and X_L represent the equivalent resistance and equivalent reactance of the line grid, respectively.

Then, the voltage deviation of the grid after distributed PV integration should be satisfied by

$$\Delta U_+ \geq \delta U_+;\ \Delta U_- \leq \delta U_- \tag{30}$$

(3) Branch Current Constraint

The current in the line must not exceed the upper limit, satisfying

$$\left| I_{ij,t} \leq \alpha_{ij,t} I_{ij,\max} \right| \tag{31}$$

where $I_{ij,t}$ denotes the branch current magnitude at time t and $I_{ij,\max}$ denotes the maximum allowable current flowing through the branch.

Additionally, according to the guidelines, the reverse power flow rate is limited to a maximum of 80%, as expressed by the following formula:

$$\lambda \leq 80\% \tag{32}$$

The calculation of the reverse power flow rate is given by the following formula:

$$\lambda = \frac{P_D - P_L}{S_e} \times 100\% \tag{33}$$

where P_D denotes the active power of distributed PV; P_L denotes the equivalent load active power, i.e., the pure load power excluding distributed PV output; and S_e denotes the power limit of electrical equipment such as transformers or lines.

4.3. Rigid Indicator Verification

After obtaining the bearing capacity results through optimization evaluation as described in Section 4.1, a short-circuit current verification is performed under the most severe scenario. If the verification passes, the bearing capacity assessment is completed. Instead, if it fails, the bearing capacity value will be updated to the limit value of the non-compliant indicator.

After integrating distributed PV into the grid, the short-circuit current should comply with the following requirements:

$$I_{xz} > I_m \tag{34}$$

where I_m denotes the short-circuit current of the system bus and I_{xz} denotes the short-circuit current limit.

4.4. Model Solving

This paper uses a sequential optimization algorithm to solve the problem because the three objective functions of the proposed distributed photovoltaic multi-power supply capacity assessment method have clear priorities.

Firstly, Objective 1 is to maximize the sum of the distributed PV capacity connected to each grid node. The purpose of this article is to determine the maximum carrying capacity of distributed PV, so this objective has the highest priority.

Secondly, Objective 2 is to maximize system static voltage stability. Generally speaking, system static voltage stability shows a trend of increasing and then decreasing with increasing PV capacity. The capacity calculated by Objective 1 will generally fall within the decreasing trend. Using the distributed PV capacity obtained by Objective 1 as the lower bound, we continue optimizing to meet safety requirements.

Finally, regarding Objective 3, economic efficiency primarily focuses on minimizing line losses. This objective is relatively unimportant. Minimizing line losses is sufficient, provided that Objectives 1 and 2 are met.

5. Evaluation Process of Distributed Photovoltaic Capacity Bearing Capacity

In summary, the evaluation process of distributed photovoltaic capacity bearing capacity can be broadly divided into two major phases: the typical scenario generation phase and the bearing capacity assessment phase. The specific workflow is illustrated in Figure 3 below.

In the typical scenario generation phase, firstly, the parameters of the photovoltaic Beta distribution and the load normal distribution are determined based on photovoltaic and historical load data, respectively. Then, the copula function is introduced to determine the joint distribution of PV and load, with joint distribution parameters estimated via maximum likelihood estimation. Based on this joint distribution, massive load and PV scenarios are generated by Latin Hypercube Sampling. The variable-weight K-Means clustering method is employed to generate representative scenarios—that is, load and PV output curves. These curves serve as the benchmark for subsequent sequential solutions in distributed PV bearing capacity assessment.

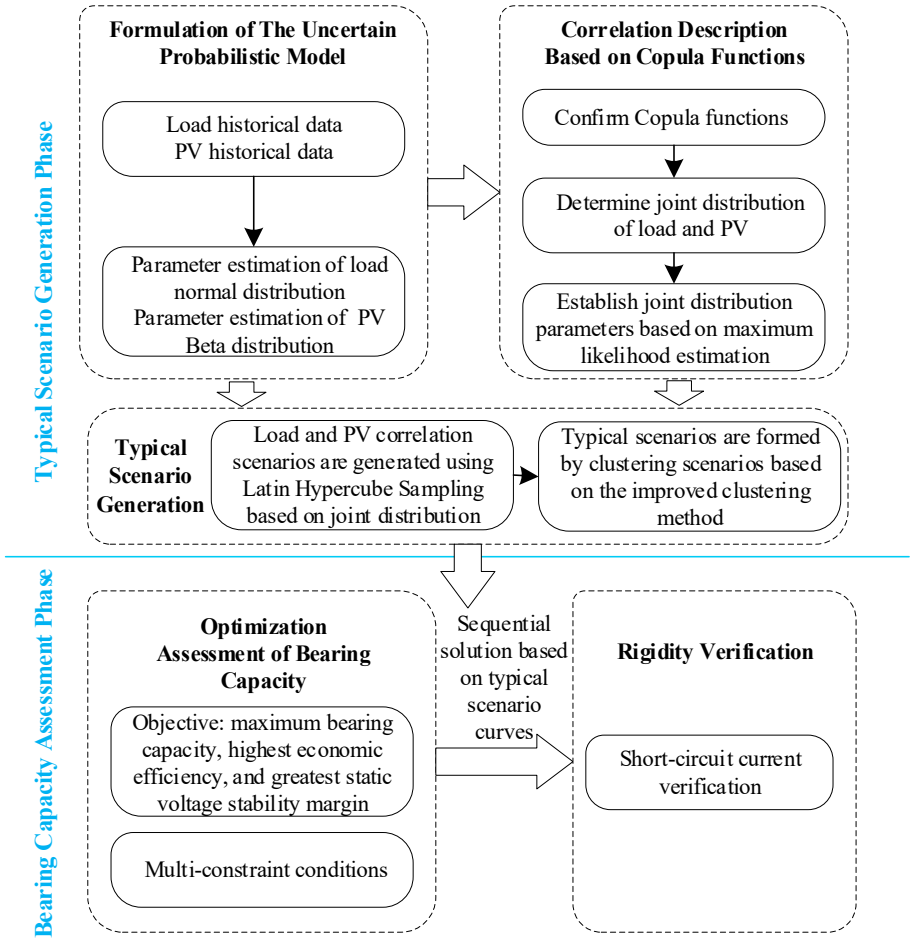


Figure 3. Evaluation Process of Distributed Photovoltaic Capacity Bearing Capacity.

In the bearing capacity assessment phase, the distributed PV bearing capacity assessment model is established with the objectives of maximizing distributed PV hosting capacity, achieving the highest economic efficiency, and ensuring the greatest static voltage stability of the system after PV integration. Sequential solutions are performed based on each time point within each typical scenario described above. The photovoltaic bearing capacity of the grid is defined by the maximum permissible distributed PV bearing capacity under the most severe scenario at its most critical time point.

6. Simulation Analysis

6.1. Case Study Introduction

(1) Grid Topology

The simulation analysis in this paper is based on the modified IEEE 33-node system, and the system structure is shown in Figure 4. In the figure, arrows and numbers indicate load locations and notes, respectively. According to the guidelines, the permissible voltage deviation at nodes ranges from 0.93 to 1.07 p.u., and the maximum allowable power flow for lines is 5.5 MW.

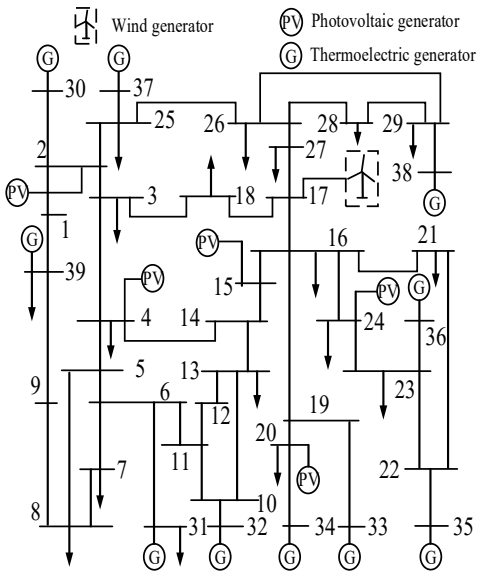


Figure 4. Modified IEEE 33-Bus System.

(2) PV and Load Data Simulation

To enhance the practicality of the case study, the example in this paper uses measured data from 16 load nodes and 8 photovoltaic sites in a distribution network in Gansu. The period is 1 h, and the time span is from 1 June to 31 August 2023 and 2024 (summer). A total of 92 data samples are collected at each time point (30 June, 31 July, and 31 September). The Beta distribution parameters of photovoltaic output and the normal distribution parameters of load output are estimated for each time point, as shown in Figures 5 and 6. Based on this, scenario design and subsequent case analysis are carried out.

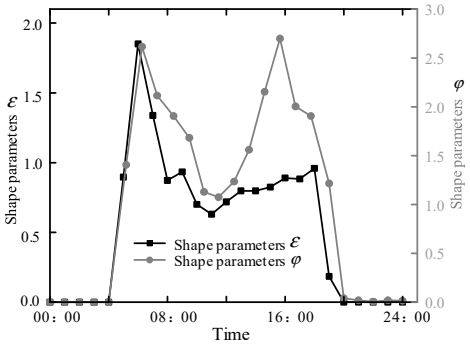


Figure 5. Photovoltaic Beta Distribution Parameter Estimation.

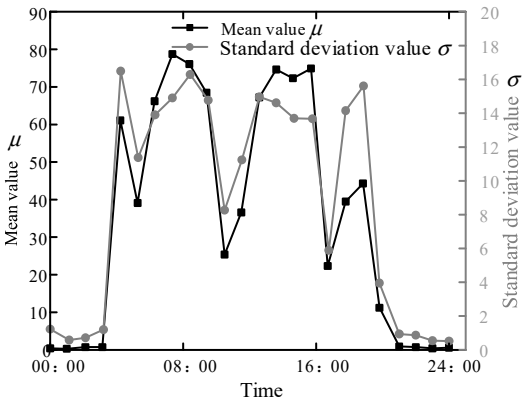


Figure 6. Parameter Estimation of Beta Distribution for Photovoltaic Output.

6.2. Analysis of the Impact of Static Voltage Stability on Distributed PV Bearing Capacity

The static voltage stability of the system is calculated under initial load and photovoltaic conditions, as shown in Figure 7.

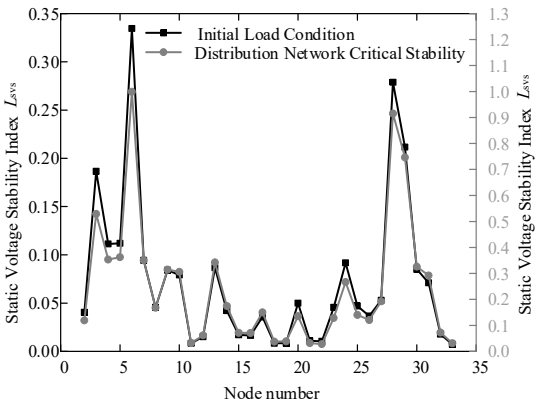


Figure 7. L_{SVS} value of each node.

As shown in Figure 7, node 6 and node 28 exhibit the highest L_{SVS} values of all the nodes, which are the static voltage stability weak nodes in this system.

When the net power load at each node of the distribution network increases proportionally, the L_{SVS} value at node 6 reaches 1 first, followed by node 28. This indicates that voltage instability occurs first at node 6, followed by node 8. Therefore, the constraining effects of these two nodes should be given priority consideration in distributed PV bearing capacity assessment.

(1) The impact of connecting photovoltaic capacity

Taking node 6 as an example, the influence of different connecting capacities on static voltage stability is analyzed. The L_{SVS} values at node 6 are calculated under three scenarios—initial load conditions, connecting a 1 MW load at node 6, and connecting a 5 MW load at node 6—as shown in Figure 8.

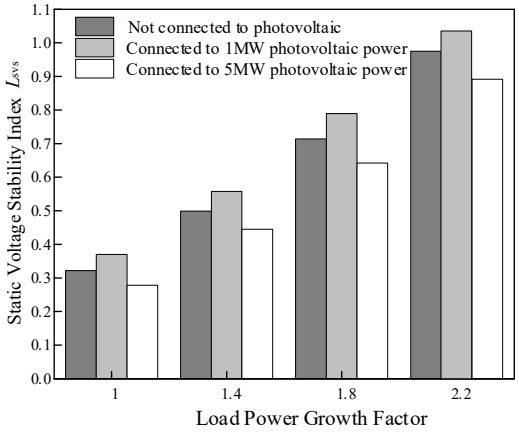


Figure 8. The impact of connecting photovoltaic capacity.

As shown in Figure 8, after connecting photovoltaic at node 6, the load power margin significantly increases. Moreover, within a certain capacity range, the greater the photovoltaic connection capacity, the more pronounced the improvement effect. Because, in a radial network, the greater the load power of a node, the more severe the voltage drop becomes, resulting in a higher L_{SVS} value. Therefore, connecting the appropriate photovoltaic capacity in the radial network can increase the voltage amplitude at the end of the

line, thereby enhancing the static voltage stability margin. However, as the distributed PV capacity continues to increase, reverse power flow occurs in the grid, causing the voltage at the end of the grid to rise and ultimately reducing the static voltage stability margin of the system. This observation is consistent with the conclusions derived from the aforementioned theoretical analysis.

(2) The impact of the connection location

Taking the example of connecting identical distributed PV capacities at nodes 6, 11, and, 33, the static voltage stability indicators for the system were calculated as shown in Figure 9.

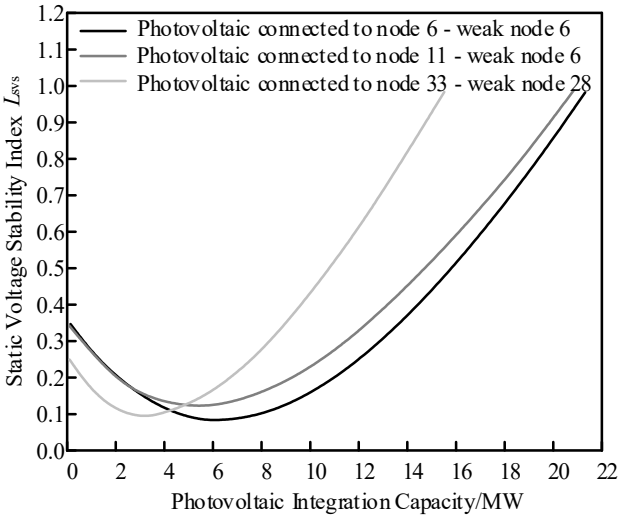


Figure 9. The impact of the connection location.

As shown in Figure 9, when distributed PV is connected at nodes 6 and 11, the static voltage stability of the system is determined by the L_{SVS} value of node 6. But when the distributed PV is connected at node 33, the system′s static voltage stability is decided by the L_{SVS} value of node 28. This demonstrates that after distributed PV is connected to the grid, the system′s static voltage stability weak points will vary under different connection schemes. Therefore, during optimizing solutions, care must be taken to avoid consistently using the L_{SVS} value of the initial weak point as the L_{SVS} value of the system, which would lead to deviations in the bearing capacity assessment.

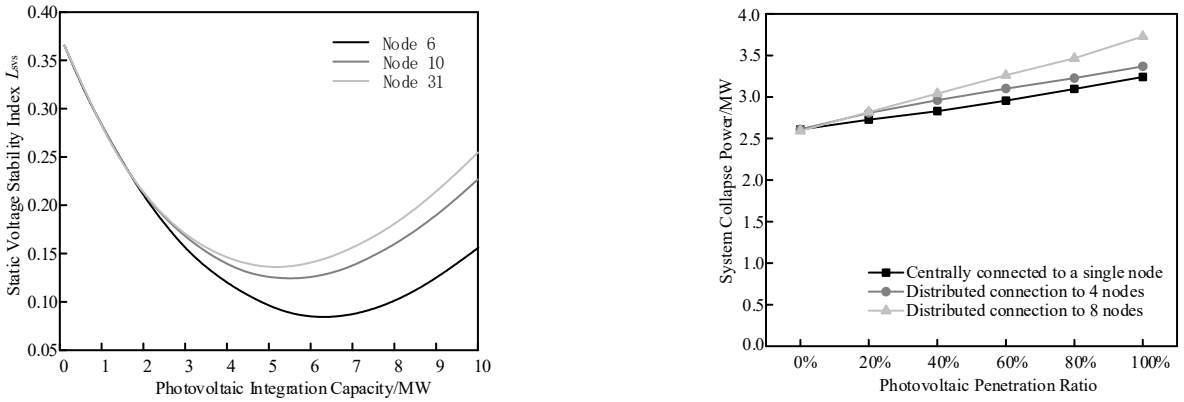
Meanwhile, different PV connection location schemes significantly influence the distributed PV bearing capacity. The following three cases are designed for comparative analysis:

Case 1: Distributed PV is permitted to connect only to a single centralized node. The simulation centralized connections to node 6, node 10, or node 11 individually.

Case 2: Distributed PV is permitted to connect to four nodes in a dispersed manner. The simulated node set is {6, 10, 11, 28}.

Case 3: Distributed PV is permitted to connect to eight nodes in a dispersed manner. The simulated node set is {4, 6, 10, 11, 15, 18, 22, 28}.

The simulation results for the three cases are shown in Figure 10.



(**a**) The simulation results of centralized access to different nodes (**b**) The simulation results for the three cases

Figure 10. The impact of different access schemes.

As shown in Figure 10, when distributed PV is integrated at the same node, the maximum bearing capacity occurs at node 6. This shows that integrating distributed PV at the initial weak point allows the power grid to host more distributed PV, because the initial weak point typically experiences heavy load and low terminal voltage. The integration of distributed PV at this location can directly alleviate the terminal voltage issue.

When distributed PV is connected to different nodes in a dispersed manner, the improvement in voltage stability is relatively more effective compared to concentrated integration, because this access method effectively reduces the overall net load of the distribution network. The more dispersed the integration locations are, the more uniformly the net load is reduced at each node, resulting in better voltage improvement effects, a higher PV capacity inflection point as defined in Formula (11), and, ultimately, a greater bearing capacity for distributed PV.

6.3. Analysis of the Impact of Source–Load Correlation on Distributed PV Bearing Capacity

Based on the measured data, the correlation coefficient ρ between PV output and active load power is calculated, as shown in Figure 11.

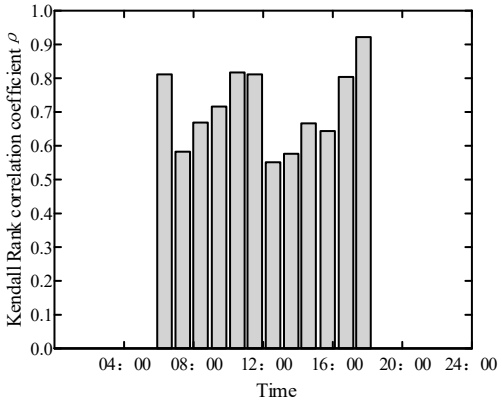


Figure 11. Correlation Coefficient between Photovoltaic Output and Load Power.

Figure 11 reveals a strong correlation between photovoltaic output and load power.

This paper presents two case studies for simulation analysis, as follows:

Case 1: Based on the PV Beta distribution and load normal distribution functions, parameters are estimated via historical data, and load and PV output data are created by sampling methods.

Case 2: Based on the copula function correlation analysis method proposed in this paper, parameters are estimated from historical data, and sampling methods are applied to generate load and PV output data.

In both cases, the model proposed in Section 4 was employed to evaluate the distributed PV bearing capacity. The distinction lies in the approach of sequential solutions: Case 2 utilized typical curves generated by considering source–load correlation, while Case 1 employed curves generated without considering such correlation.

The correlation coefficients between photovoltaic and load data under the two cases are shown in the figure below.

As shown in Figure 12, the load and PV data generated using the copula function correlation analysis method proposed in this paper better align with actual conditions.

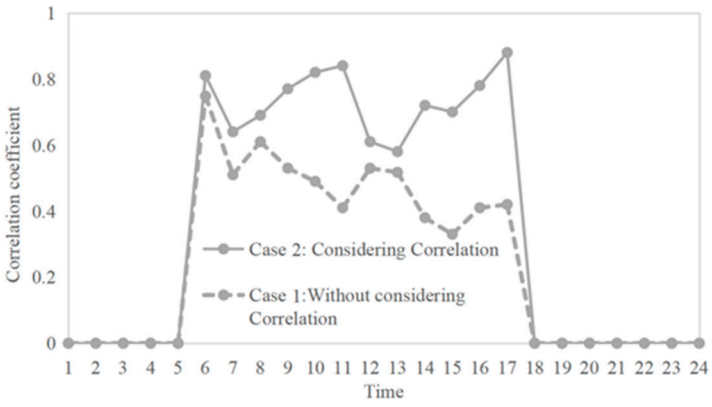


Figure 12. Correlation coefficient considering correlation and correlation coefficient not considering correlation.

To analyze the impact of correlations between photovoltaic output and load random variables on PV bearing capacity, the following two scenarios are provided for comparative analysis.

Scenario 1: The distributed PV bearing capacity is evaluated without considering the correlation between PV and load. That is, typical scenarios of PV and load are generated without accounting for their correlation, and the assessment is performed based on these scenarios.

Scenario 2: The distributed PV hosting capacity is evaluated considering the correlation between PV and load. That is, typical scenarios of PV and load are generated, accounting for their correlation, and the assessment is conducted based on these scenarios.

The distributed PV bearing capacities under the two scenarios are shown in Figure 13.

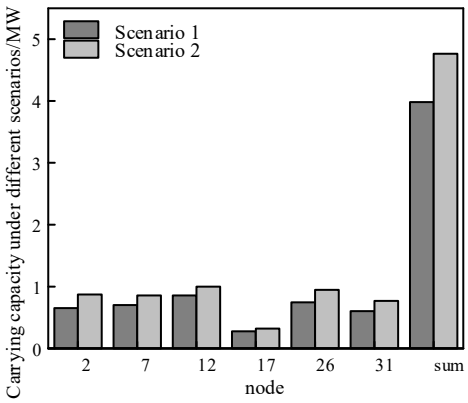


Figure 13. Bearing capacity assessment considering correlation and bearing capacity assessment without considering correlation.

As shown in Figure 13, the calculated PV bearing capacity under Scenario 2 is higher at each node, with a total value of 4.8 MW. Compared to Scenario 1, the calculation results increased by 0.72 MW. This is because when the connected photovoltaic system and the load exhibit a correlation, the load can promptly absorb the photovoltaic output, thereby increasing the grid′s capacity to accommodate distributed photovoltaic.

7. Conclusions

Addressing the issue of distributed PV bearing capacity assessment, this paper proposes a distributed PV bearing capacity assessment method by considering key factors such as static voltage stability and photovoltaic–load coupling. The main conclusions are as follows:

(1) When a centralized integration scheme is adopted, connecting distributed PV to the initial weak point allows for higher PV bearing capacity. The reason is that the initial weak point is characterized by a heavy load and low terminal voltage, and integrating PV at this location can improve the terminal voltage issue.
(2) A distributed integration scheme can accommodate more distributed PV compared to a centralized approach. Moreover, the greater the number of nodes involved in distributed integration, the more significant the improvement in hosting capacity.
(3) The assessment result for distributed PV bearing capacity considering source–load correlation is higher than that ignoring such correlation. This is attributed to the positive correlation between source and load: during periods of high PV output, the load power is also substantial, thereby enhancing distributed PV hosting capacity.

8. Discussion

In fact, the carrying capacity of distributed photovoltaics is related to many factors. In this article, we not only consider the factors in the "Guidelines for Evaluating the Carrying Capacity of Distributed Power Sources Connected to the Grid" (such as heavy overload of power flow, short-circuit current, voltage exceeding limits, etc.) but also consider static voltage stability, source–load correlation, and line loss economy, making the assessment of distributed photovoltaic carrying capacity more suitable for the current scenario where the proportion of distributed photovoltaic access is increasing.

However, in reality, distributed PV systems employing different grid connection control strategies have varying support capabilities for the system′s static voltage stability. For example, in constant power factor control mode, the inverter operates at a set power factor (e.g., PF = 1.0, meaning only active power is generated) and provides no voltage support to the grid.

In constant voltage control mode, the inverter monitors the grid-connection point voltage and maintains voltage stability by adjusting the reactive power. When the voltage rises, it absorbs reactive power; when the voltage drops, it generates reactive power, which contributes to system static voltage stability.

In active power derating control mode, when the grid-connection point voltage is excessively high, the active power output is proactively reduced, which can alleviate steady-state voltage overshoots but provides relatively insufficient support for static voltage stability.

Due to the complex coupling between distributed PV grid-connection control strategy parameter setting and load capacity assessment, this study assumes that distributed PV systems employ a constant power factor control mode. Subsequent research will focus on the impact of distributed grid-connection control strategies on load capacity assessment.

Author Contributions: Conceptualization, Y.S. and Y.L. (Yalong Li); methodology, Z.W. and Y.L. (Yongcheng Liu); validation, Y.S. and Z.W.; investigation, Y.L. (Yongcheng Liu); resources, Z.W.; data curation, Y.S.; writing—original draft preparation, Y.S., Y.L. (Yalong Li) and Y.J.; writing—review and editing, Y.J., Y.S. and Y.L. (Yalong Li). All authors have read and agreed to the published version of the manuscript.

Funding: This research received no external funding.

Data Availability Statement: The raw data supporting the conclusions of this article will be made available by the authors on request.

Conflicts of Interest: Author Yalu Sun, Zhou Wang, Yongcheng Liu was employed by the Economic and Technological Research Institute of State Grid Gansu Electric Power Company. The remaining authors declare that the research was conducted in the absence of any commercial or financial relationships that could be construed as a potential conflict of interest.

Appendix A

The derivation process of the static voltage stability index is as follows, based on Equation (A1).

$$U_{am}\angle\delta_{am} = U_b\angle\delta_b + \frac{(R_{am\text{-}b} + jX_{am\text{-}b})(P_{am\text{-}b} - jQ_{am\text{-}b})}{U_b\angle -\delta_b} \tag{A1}$$

In the equation, U_{am} and U_b denote the voltages of node *am* (the *m*-th node connected to node *b*) and node *b*, respectively; δ_{am} and δ_b denote the phase angles of node *am* and node *b*, respectively; $R_{am\text{-}b}$ and $X_{am\text{-}b}$ denote the resistance and reactance of branch *am-b* (the *m*-th branch connected to node *b*), respectively; and $P_{am\text{-}b}$ and $Q_{am\text{-}b}$ denote the active power and reactive power of branch *am-b* (the *m*-th branch connected to node *b*), respectively.

The amplitudes on both sides of the formula are equal, so we can obtain

$$\begin{aligned} U_{am} &= U_b + \tfrac{(R_{am\text{-}b}+jX_{am\text{-}b})(P_{am\text{-}b}-jQ_{am\text{-}b})}{U_b} \\ \Rightarrow U_{am} &= U_b + \tfrac{P_{am\text{-}b}R_{am\text{-}b}+Q_{am\text{-}b}X_{am\text{-}b}+j(P_{am\text{-}b}X_{am\text{-}b}-Q_{am\text{-}b}X_{am\text{-}b})}{U_b} \\ \Rightarrow U_{am}^2 &= \left(U_b + \tfrac{P_{am\text{-}b}R_{am\text{-}b}+Q_{am\text{-}b}X_{am\text{-}b}}{U_b}\right)^2 + \left(\tfrac{P_{am\text{-}b}X_{am\text{-}b}-Q_{am\text{-}b}R_{am\text{-}b}}{U_b}\right)^2 \end{aligned} \tag{A2}$$

Equation (A2) shows the relationship between the voltage at node *am* (the *m*-th node connected to node *b*) and the power, impedance, and voltage of branch *am-b* (the *m*-th branch connected to node *b*).

In order to simplify the form of the formula, let

$$\begin{cases} M = P_{am\text{-}b}R_{am\text{-}b} + Q_{am\text{-}b}X_{am\text{-}b} \\ N = P_{am\text{-}b}X_{am\text{-}b} - Q_{am\text{-}b}R_{am\text{-}b} \end{cases} \tag{A3}$$

According to Kirchhoff's law, the sum of the power of all branches connected to node *b* is equal to the injected power of node *b*, and the branch power is inversely proportional to the impedance, so

$$P_{am\text{-}b} + jQ_{am\text{-}b} = \frac{\frac{1}{R_{am\text{-}b} + jX_{am\text{-}b}}}{\sum_{k=1}^{K} \frac{1}{R_{ak\text{-}b} + jX_{ak\text{-}b}}}(P_b + jQ_b) \tag{A4}$$

Expand Equation (A4). Considering the complexity of the formula, we can simplify $P_{am\text{-}b}$ and $Q_{am\text{-}b}$ as a function of the node injection power P_b and Q_b, which is

$$\begin{cases} M = f_p(P_b, Q_b)R_{am\text{-}b} + f_q(P_b, Q_b)X_{am\text{-}b} \\ N = f_p(P_b, Q_b)X_{am\text{-}b} - f_q(P_b, Q_b)R_{am\text{-}b} \end{cases} \tag{A5}$$

Substitute Equation (A5) into Equation (A2) and expand it to obtain

$$\begin{aligned} U_{am}^2 &= \left(\frac{U_b^2+M}{U_b}\right)^2 + \left(\frac{N}{U_b}\right)^2 \\ U_b^4 &- (U_{am}^2 - 2M)U_b^2 + M^2 + N^2 = 0 \end{aligned} \tag{A6}$$

From the above formula, we can see that the voltage equation of node b satisfies the quadratic relationship. If the voltage of node b is stable, it means that Equation (A6) has a real number solution. Similarly, if Equation (A6) has a real number solution, it means that there is voltage at node b under any operating state, and the voltage of node b is stable. This shows that Equation (A6) has a real number solution, and the voltage stability of node b is equivalent. According to the condition that the binary linear function has a solution, we can know that

$$\begin{aligned} &\Delta = b^2 - 4ac \geq 0 \\ &\Rightarrow \Delta = \left(U_{am}^2 - 2M\right)^2 - 4\left(M^2 + N^2\right) \geq 0 \\ &\Rightarrow \Delta = U_{am}^4 - 4MU_{am}^2 - 4N^2 \geq 0 \\ &\Rightarrow U_{am}^4 \geq 4\left(MU_{am}^2 + N^2\right) \\ &\text{because} U_{am}^4 > 0, \\ &\frac{4\left(MU_{am}^2+N^2\right)}{U_{am}^4} \leq 1 \end{aligned} \tag{A7}$$

Therefore, the voltage stability index $L_{\text{SVS,am-}b}$ of node b based on branch am-b can be defined as

$$L_{\text{SVS},am\text{-}b} = \frac{4[N^2 + MU_{am}^2]}{U_{am}^4} \tag{A8}$$

The smaller the value of this indicator, the more stable the voltage. When $L_{\text{SVS},am\text{-}b} = 1$, the static voltage of the system becomes unstable.

The static voltage stability of node b is determined by the worst absolute value of all power supply branches. Then, the voltage stability index of node b, $L_{\text{SVS},b}$, is

$$L_{\text{SVS},b} = \max_{b=1:K}(L_{\text{SVS},ak\text{-}b}) \tag{A9}$$

The smaller $L_{\text{SVS},b}$ is, the larger the static voltage stability margin of node b. When $L_{\text{SVS},b}$ is greater than 1, the voltage of node b begins to become unstable.

Similarly, the static voltage stability of the entire system is determined by the worst node. Therefore, the static voltage stability of the entire system $L_{\text{SVS},s}$ is

$$L_{\text{SVS},s} = \max_{k}(L_{\text{SVS},k}) \tag{A10}$$

References

1. Suchithra, J.; Rajabi, A.; Robinson, D.A. Enhancing PV hosting capacity of electricity distribution networks using deep reinforcement learning-based coordinated voltage control. *Energies* **2024**, *17*, 5037. [CrossRef]
2. Santos, B.L.; Barbosa, D.; Barros, L.S.; Moreira, F.A. Photovoltaic hosting capacity maximization of low-voltage distribution systems based on search of optimal power factor for interface inverters through particle swarm optimization. *J. Control Autom. Electr. Syst.* **2023**, *34*, 1260–1271. [CrossRef]
3. Karadeniz, A.; Balci, M.; Hocaolu, M.H. Improvement of PV unit hosting capacity and voltage profile in distorted radial distribution systems via optimal sizing and placement of passive filters. *Electr. Eng.* **2023**, *105*, 2185–2198. [CrossRef]

4. Fang, J.; Li, P.; Yu, H.; Yu, L.; Ji, H.; Liu, Y.; Zhao, J.; Lei, Y. Matrix-based analytical calculation method for distributed photovoltaic integration region in active distribution network. *Electr. Power Autom. Equip.* **2025**, *45*, 3–11+19.
5. Li, H.; Zhao, F.; Shu, Z.; Chen, L.; Tong, H.; Bao, G. Enhancement optimization model for distributed photovoltaic hosting capacity considering multiple adjustment methods. *Power Demand Side Manag.* **2025**, *27*, 82–87.
6. Deng, M.; Chen, Y.; Bai, Z. Quantification method for distributed photovoltaic hosting capacity of distribution networks based on static voltage stability margin. *J. Shanghai Jiaotong Univ.* **2024**, *357*, 1–25.
7. Zhang, Q.; Li, N.; Lin, C.; Wu, J.; Zhang, W.; Liu, H. Research and application of distributed photovoltaic flexible participation in power grid peak shaving technology based on the concept of grading and collaboration. *Shandong Electr. Power* **2025**, *52*, 46–53.
8. Yao, S.; Zhao, Z.; Qin, H. Analysis of Technology for Improving Bearing Capacity of Distribution Networks with High Penetration of Distributed Photovoltaics. *Electr. Power Equip. Manag.* **2025**, *01*, 19–21.
9. Zhao, H.; Hu, Z.; Wei, W.; Wen, K. A method to improve the carrying capacity of a distributed photovoltaic power distribution network considering correlation. *Power Syst. Prot. Control* **2025**, *53*, 37–46.
10. Lü, D. Distributed photovoltaic carrying capacity assessment considering source load uncertainty. *J. Shanghai Univ. Electr. Power* **2024**, *40*, 579–586.
11. Wang, F.; Xu, J.; Su, N.; Niu, H.; Yuan, J.; Men, P. Probability evaluation method of distributed photovoltaic carrying capacity under risk suppression in new power system. *Electr. Power* **2025**, *58*, 33–44.
12. Yadav, A.; Kishor, N.; Negi, R. Voltage profile analysis at planning and operational stages with allowable PV hosting capacity. *IET Renew. Power Gener. (RPG)* **2024**, *18*, 16. [CrossRef]
13. Zhao, H.; Hu, Z.; Wei, W.; Wen, K. A comprehensive evaluation method of distributed photovoltaic carrying capacity of distribution network based on SAO-VIKOR. *J. North China Electr. Power Univ. (Nat. Sci. Ed.)* **2025**, 1–10.
14. Liang, J.; Tian, X.; Bi, L. A model for estimating the ultimate bearing capacity of wide-area distributed photovoltaic access grid. *Electron. Des. Eng.* **2024**, *32*, 147–151.
15. Koirala, A.; Van Acker, T.; Hashmi, M.U.; D'hulst, R.; Van Hertem, D. Chance-Constrained Optimization Based PV Hosting Capacity Calculation Using General Polynomial Chaos. *IEEE Trans. Power Syst. A Publ. Power Eng. Soc.* **2023**, *39*, 2284–2295. [CrossRef]
16. Noman, S.; Lauri, K.; Victor, A.; Kamran, D.; Muhammad, J.; Oleksandr, H.; Argo, R.; João, M. Enhancing PV hosting capacity and mitigating congestion in distribution networks with deep learning based PV forecasting and battery management. *Appl. Energy* **2024**, *372*, 123770.
17. Li, J.; Bai, Y.; Wang, X.; Song, Y.; Zhou, B.; Guo, Y.; Li, L. A calculation method for PVs' safe and economic carrying capacity that consider transmission and distributed network coordination. *Electr. Power Constr.* **2025**, *46*, 113–121.
18. Zheng, Y.; Zhou, K.; Yang, Y.; Diao, H.; Hua, L.; Wang, R.; Liu, K.; Guo, Q. Robust Assessment Method for Hosting Capacity of Distribution Network in Mountainous Areas for Distributed Photovoltaics. *Energies* **2025**, *18*, 2394. [CrossRef]
19. Jiang, W.; Du, Z.; Zhou, W.; Lin, X. Photovoltaic hosting capacity assessment of a distributed network based on an improved holomorphic embedding load flow method and stochastic scenario simulation. *J. Renew. Sustain. Energy* **2024**, *16*, 14. [CrossRef]
20. Men, M.; Zhao, R.; Zhang, J.; Wang, P.; Zhang, Q. Evaluation of distributed photovoltaic hosting capacity of distribution networks based on improved simulated annealing-particle swarm optimization. *J. Zhejiang Univ. (Eng. Sci.)* **2024**, *58*, 1255–1265.
21. Bai, Y. Coordinated Configuration. Coordinated Configuration Method of Medium—and Low—Voltage Distributed Network with Distributed Photovoltaic Considering Influence of Regulation and Trading Modes. Master's Thesis, North China Electric Power University, Beijing, China, 2024.
22. Jaramillo-Leon, B.; Zambrano-Asanza, S.; Franco, J.F.; Soares, J.; Leite, J.B. Allocation and smart inverter setting of ground-mounted photovoltaic power plants for the maximization of hosting capacity in distribution networks. *Renew. Energy* **2024**, *223*, 119968. [CrossRef]
23. Mabrook, M.M.; Donkol, A.A.; Mabrouk, A.M.; Hussein, A.I.; Barakat, M. Enhanced the Hosting Capacity of a Photovoltaic Solar System Through the Utilization of a Model Predictive Controller. *IEEE Access* **2024**, *12*, 12. [CrossRef]
24. Li, C.; Wang, Y.; Zhu, X.; Qi, X.; Guan, X.; Li, J.; Chang, Z.; Bai, Y.; Li, H. Copula function based on second-order cone relaxation optimal power flow and robust weighted K-Means method for PV carrying capacity evaluation. *Adv. Technol. Electr. Eng. Energy* **2025**, *44*, 74–88.
25. Liu, X. Research on the Evaluation of Distributed Photovoltaic Hosting Capacity in Distribution Networks Based on Coupled Meteorological Factors. Master's Thesis, Guangdong University of Technology, Guangzhou, China, 2025.
26. Han, N. Evaluation and Enhancement Method of the Distributed Photovoltaic Carrying Capacity Based on Combined Energy Router. Master's Thesis, Northeast Electric Power University, Jilin, China, 2025.
27. Eftekharnejad, S.; Vittal, V.; Heydt, G.T.; Keel, B.; Loehr, J. Small signal stability assessment of power systems with increased penetration of photovoltaic generation: A Case Study. *IEEE Trans. Sustain. Energy* **2013**, *4*, 960–967. [CrossRef]

28. Ayaz, M.S.; Malekpour, M.; Azizipanah-Abarghooee, R.; Karimi, M.; Terzija, V. Probabilistic photovoltaic generation and load demand uncertainties modelling for active distribution networks hosting capacity calculations. *Int. J. Electr. Power Energy Syst.* **2024**, *159*, 10.
29. Zhang, Y.; Wei, X.; Feng, K.; Shi, S.; Meng, Z.; Liang, Y. Charging and discharging strategies of independent energy storage for distribution grid side considering distributed PV carrying capacity. *Electr. Power* **2024**, *57*, 111–117.
30. Ming, M.; Zhou, N.; Gao, L.; Liu, Y.; Li, C.; Cui, M.; Ma, H. Analysis, evaluation and application of distributed photovoltaic carrying capacity in active distribution networks. *Distrib. Util.* **2023**, *40*, 35–53.
31. Wang, H.; Xu, Y.; Xu, D.; Luo, Z.; Li, Y.; Su, H.; Peng, X. Evaluation of distributed rooftop photovoltaic hosting capacity in distribution networks based on high definition satellite map images. *Guangdong Electr. Power* **2023**, *36*, 105–113.
32. Wang, Y.; Wang, T.; Yue, Y.; Wang, H.; Chen, C.; Li, G. Flexible resource collaborative planning to enhance the capacity of distributed photovoltaic. *Power Syst. Clean Energy* **2023**, *39*, 116–126.
33. Yang, Z.; Yang, F.; Min, H.; Hu, W.; Lei, Y.; Liu, Y. Distributed PV hosting capacity robust assessment of AC/DC hybrid distribution network considering demand response. *High Volt. Eng.* **2024**, *50*, 83–92.
34. Wang, Q.; Yao, L.; Sheng, W.; Xu, Y.; Liu, K.; Cheng, F. Enhancement method for distributed photovoltaic hosting capacity of distribution network based on chance-constrained programming. *Autom. Electr. Power Syst.* **2023**, *47*, 132–141.
35. *GB/T 33593-2017*; Technical Requirements for Grid Connection of Distributed Resources. National Standard of the People's Republic of China: Beijing, China, 2017.

Disclaimer/Publisher's Note: The statements, opinions and data contained in all publications are solely those of the individual author(s) and contributor(s) and not of MDPI and/or the editor(s). MDPI and/or the editor(s) disclaim responsibility for any injury to people or property resulting from any ideas, methods, instructions or products referred to in the content.